ADVANCED INTELLIGENT SYSTEMS
Open Access
www.advintellsyst.com

A Robotic Urinary Bladder Enabling Volume Monitoring and Assisted Micturition

Izadyar Tamadon, Michele Ibrahimi, Federica Semproni, Veronica Iacovacci, and Arianna Menciassi**

The urinary bladder is considered a highly complex organ, capable not only of storing urine but also of sensing intra-vesical volume and dynamically expanding and contracting. Consequently, fully replicating its functions following radical cystectomy remains a significant technological challenge. Hereinafter, an implantable robotic bladder is presented that can change shape and expand its internal volume up to 400 mL, based on the amount of urine collected from kidneys, and monitor the volume in real-time. It can apply on-demand mechanical compression to assist urination, by means of an origami-designed enclosure, coupled to miniaturized mechatronic components. In vitro characterization in a human phantom is demonstrated, and volume monitoring is validated following a realistic filling routine. The tests demonstrate successful expansions for collecting urine, with an average volume reconstruction error of 8.4 ± 6.1 mL, and then 99% of the volume is voided in less than 2 min. The work paves the way for developing active robotic solutions and reproducing bladder functions in patients with cancer and organ removal or impairment.

1. Introduction

Implantable artificial organs represent one of the most promising frontiers in the evolving field of medical robotics.[1] These remarkable devices, designed to integrate seamlessly with the human body, offer the potential to transform the lives of individuals affected by organ failure in ways that were once thought impossible.[2] This flourishing domain promises not only to alleviate the persistent shortage of donor organs but also to push the boundaries of our understanding of artificial systems within the human body.[3] The potential applications of artificial organs are as vast as the challenges they pose. Artificial urinary bladders stand out among these applications, considering their profound impact on patients' independence, emotions, and social life.[4]

The advent of artificial urinary bladders represents a significant leap forward in urology, offering a novel approach that addresses the complex challenges associated with bladder dysfunctions or removal.[5] However, the development of an artificial bladder requires intricate coordination of muscle contractions in harmony with the nervous system to mimic the natural function of the urinary organ (**Figure 1**A). The bladder concepts presented in the last few decades have sparked considerable interest and excitement within the medical community, and if successfully implemented, they can promise to advance the landscape of urological care. These ingenious devices are designed to somehow mimic the natural functionality of the human urinary bladder, such as urine storing,[6–8] volume sensing,[9–14] and active voiding.[15–19] The advent of these devices can reduce the need for external catheters and pouches, thereby lowering the complications of traditional urinary diversion procedures and bowel neobladder reconstruction, which are currently the most widely used methods.[20]

However, the journey toward developing a fully implantable artificial bladder remains in its early research stages, with many challenges yet to be overcome. These challenges can be summarized as following: the need for compact and implantable electronics capable of monitoring the bladder status, the ability of the device to expand effectively during filling, and the production of the required pressure for micturition. Each of these issues presents significant hurdles that must be addressed to develop a fully implantable artificial bladder that can reliably replicate the functions of a natural bladder.

The present study proposes a novel robotic structure for patients requiring radical cystectomy caused by muscle-invasive bladder cancer,[21] which is the tenth most common

I. Tamadon
Faculty of Engineering Technology
University of Twente
Drienerlolaan 5, 7522 NB Enschede, Netherlands
E-mail: i.tamadon@utwente.nl

M. Ibrahimi, F. Semproni, V. Iacovacci, A. Menciassi
The BioRobotics Institute
Scuola Superiore Sant'Anna
Piazza Martiri della Libertà 33, 56127 Pisa, Italy
E-mail: arianna.menciassi@santannapisa.it

M. Ibrahimi, F. Semproni, V. Iacovacci, A. Menciassi
Department of Excellence in Robotics & AI
Scuola Superiore Sant'Anna
Piazza Martiri della Libertà 33, 56127 Pisa, Italy

The ORCID identification number(s) for the author(s) of this article can be found under https://doi.org/10.1002/aisy.202500516.

© 2025 The Author(s). Advanced Intelligent Systems published by Wiley-VCH GmbH. This is an open access article under the terms of the Creative Commons Attribution License, which permits use, distribution and reproduction in any medium, provided the original work is properly cited.

DOI: 10.1002/aisy.202500516

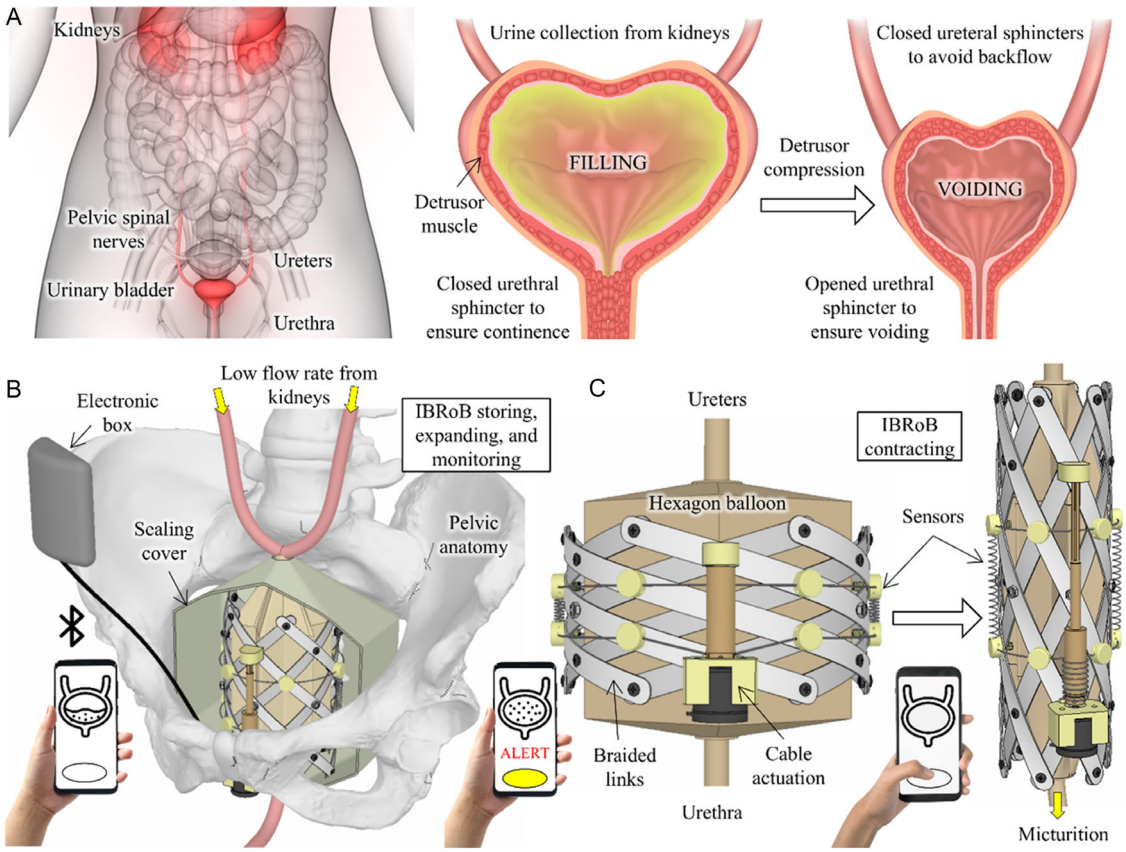

Figure 1. Illustrations of both the native bladder and the IBRoB functionality. A) The urinary system consists of kidneys, ureters, bladder, and urethra (left) (Standard license by magicmine/stock.adobe.com). The urinary bladder collects urine from the kidneys through the ureters while the bladder walls stretch and the urethral sphincter is closed (middle), then the contraction of the detrusor muscle and the relaxation of the urethral sphincter enable urine micturition (right) (Standard license by Ihor/stock.adobe.com). B) Illustration of the IBRoB implantation in the abdominal cavity, guaranteed by the anastomosis of the ureters and urethra with the native canals. C) Representation of the expanded IBRoB (end of urine collection, left) and the collapsed IBRoB (end of voiding, right). The IBRoB communicate via Bluetooth with an external app to provide the patient with feedback on the fullness status and get a command of voiding.

form of cancer worldwide.[22] The implantable braided robotic bladder (IBRoB) is designed to reshape according to its internal urine volume and to monitor the volume with an inductance sensing method (Figure 1B). To enable urine voiding, thus mimicking the natural detrusor muscles, IBRoB can apply an on-demand uniform compressive force through a cable tensioning strategy (Figure 1C). The IBRoB is designed with compact mechatronic components in such a way that it can be easily scaled to fit the anatomy of each individual patient and facilitate its implantation in lieu of the removed native bladder.

We characterized the inductance sensing and cable voiding principles in separate individual experiments. Afterwards, we evaluated the IBRoB prototype in a series of on-bench filling and voiding trials to estimate the sensing accuracy as well as the active detrusor efficiency in voiding. Finally, we demonstrated the performance of the prototype when positioned inside a human pelvis phantom with simulated abdominal organs positioned around the prototype, to replicate a realistic implanted configuration.

2. Results

The IBRoB is designed and developed to be surgically implanted in the human pelvic site in lieu of the native bladder through the anastomosis of the native ureters and urethra with the artificial ones (Figure 1B). The IBRoB is free to expand and contract to support the filling and voiding phases, while the electronics are packed in a dedicated box. The bladder expansion occurs in accordance with the amount of urine entering the bladder, while the estimated internal volume is wirelessly transferred to a paired device to provide the patient with feedback on the fullness status. Once the bladder reaches 80% of its volumetric capacity, it sends an alert to the paired device. The actuation mechanism can be activated to force the urine out of the urethra upon the patient's command (Figure 1C). Continuous feedback ensures that drainage stops only when the bladder reaches the steady-state residual volume of maximum of 10 mL. This filling-emptying cycle can be repeated to continuously store and expel urine. The real prototype is shown in **Figure 2**A, while the sealing cover has been intentionally opened to demonstrate its internal components.

© 2025 The Author(s). Advanced Intelligent Systems published by Wiley-VCH GmbH

26404567, 2026, 2, Downloaded from https://advanced.onlinelibrary.wiley.com/doi/10.1002/aisy.202500516 by Veronica Iacovacci - UNIVERSITY OF ESSEX , Wiley Online Library on [24/06/2026]. See the Terms and Conditions (https://onlinelibrary.wiley.com/terms-and-conditions) on Wiley Online Library for rules of use; OA articles are governed by the applicable Creative Commons License

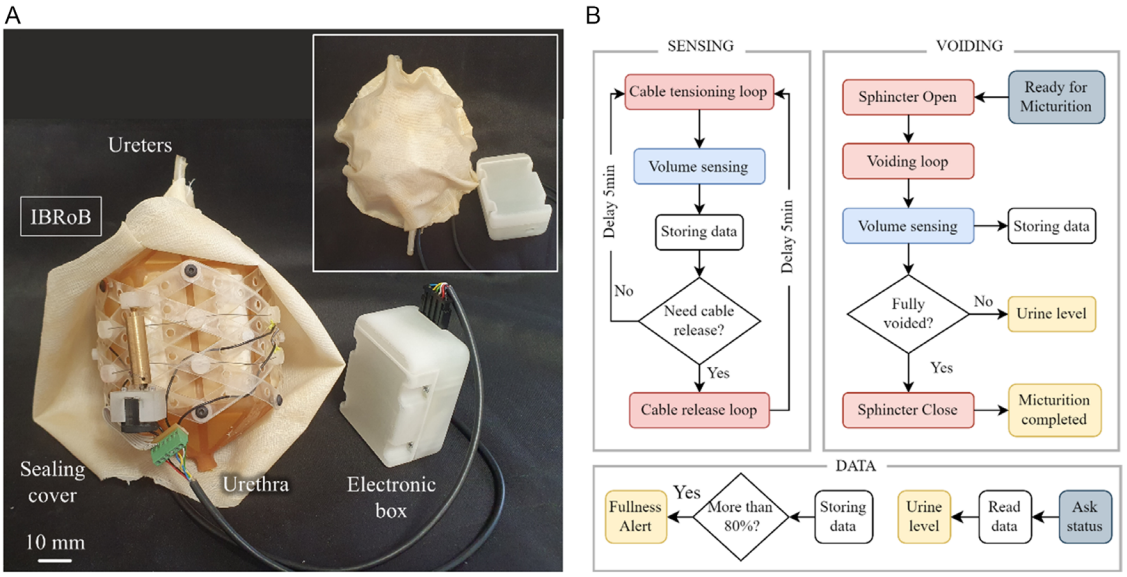

Figure 2. IBRoB prototype and its control loop. A) The opened device includes a sealing cover, a balloon and braided links, cable actuation and inductance sensing systems, and an electronic box. Inset: the device once closed for implantation. B) The control loop workflows for volume sensing, data exchange, and voiding phases. The red blocks are the actions performed by the IBRoB, the yellow blocks indicate the communications from the device to the patient, the blue block represents the sensing phase, whereas the gray blocks stand for the actions performed by the patient.

2.1. The IBRoB Design

The proposed IBRoB is composed of four sub-systems, enabling the successful functioning of the described operation: i) the IBRoB structure, constituted by a soft balloon as bladder body to store urine within a braided structure, aimed to apply a uniform pressure on the balloon during voiding; ii) a sensing system, based on inductance sensors to monitor the bladder volume; iii) a cable-based actuating mechanism to guarantee an efficient and stable contraction-expansion sequence; and iv) the control and interface electronics for a correct functioning. The IBRoB technical requirements include, i) bladder voiding pressure of 3–4 kPa;[17] ii) voiding time of less than 4 min;[23] iii) steady-state residual volume of maximum 10 mL.[23]

2.2. The IBRoB Structure

The bladder balloon shape was inspired by an origami technique that allows a guided expansion-compression-expansion cycle. In fact, a full balloon forms a hexagonal shape, while an empty balloon forms a star-like shape. The presence of folds facilitates the complete closure of the balloon and leads to nearly zero internal volume in the empty configuration (Movie S1, Supporting Information). This is crucial to avoid urine residuals after urination, which would lead to bacterial infections.[24] It is also crucial to consider the positive pressure caused during contractions toward the kidneys.[25,26] Anatomically, mucosal flaps cover the ureter's entry point, preventing urine from entering the ureters during micturition. Our solution for mimicking this functionality was based on an antireflux sphincter that prevents backflow by compressing a double-layer ureter.[27] Experimental results confirmed the backflow blocking for a full bladder and 4 kPa outlet pressure. Only a few drops (0.014 mL min^{-1}) were noted in cases with 25% overpressure (i.e., 5 kPa).

The braided structure of the IBRoB is inspired by the natural anatomy of the middle layer in the detrusor muscle structure.[28] In this layer, smooth muscles are formed in all directions like interwoven fibers, which enable uniform compression of the bladder. Similarly, our design incorporates flexible braided links that intersect to form a variable-diameter helical cylinder (Movie S2, Supporting Information). The braided structure design can transfer the actuation compression force to the balloon and fold the balloon's sides to create a star-like shape. Moreover, it works as a base structure to hold sensors. We exploited fabrication techniques that allowed for an easy integration of the braided links and the hexagon balloon. The bladder balloon and the braided links can be easily sized to reproduce a native bladder capacity and be matched with the anatomy.

2.3. The IBRoB Sensing Strategy

A proper implementation of a sensing strategy is highly requested to identify the appropriate moments of micturition. Due to the constraints imposed by the in-body conditions, sensing solutions suitable for implantable organs are very limited.[14] We have investigated inductance sensors using tension springs because of their low-power consumption, high elongation rate, and small size.[29] In the IBRoB design, two tension springs are longitudinally arranged at mid-body and opposite sides of the braided structure (**Figure 3**A) to provide a constant force useful to overcome structural friction in the filling phase while urine has a low pressure flow rate (equal to 0.5 kPa[30]). The springs are sized so that their rest length is reached in the bladder expanded condition. In this way, the averaged sensor length was used to determine the radius of the IBRoB and estimate the volume

© 2025 The Author(s). Advanced Intelligent Systems published by Wiley-VCH GmbH

26404567, 2026, 2, Downloaded from https://advanced.onlinelibrary.wiley.com/doi/10.1002/aisy.202500516 by Veronica Iacovacci - UNIVERSITY OF ESSEX , Wiley Online Library on [24/06/2026]. See the Terms and Conditions (https://onlinelibrary.wiley.com/terms-and-conditions) on Wiley Online Library for rules of use; OA articles are governed by the applicable Creative Commons License

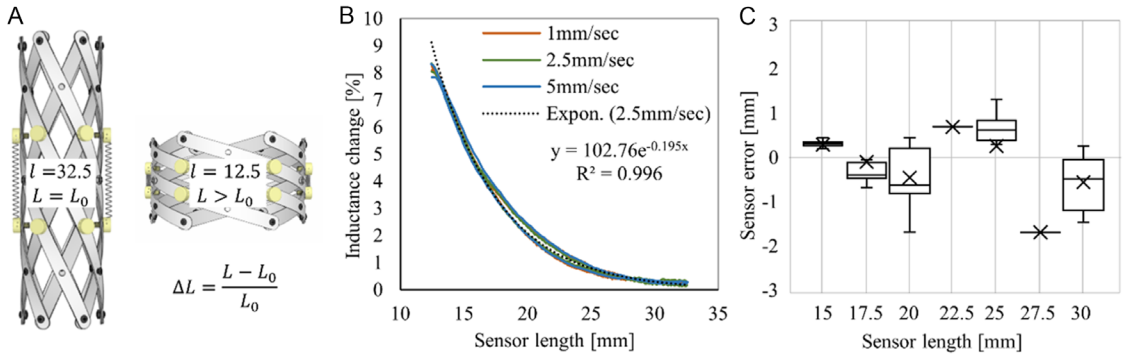

Figure 3. Sensing performance. A) The schematic representation of the sensor length (l) and the inductance changes (L). B) The sensor inductance changes with respect to the sensor length, with 3 different elongation rates. C) The sensor error with respect to the sensor length.

bladder body. As shown in Figure 3B, the sensor read-out is highly uniform with a very low hysteresis (equal to 0.7%) during all elongation-shortening cycles and variable elongation rates. We considered an exponential curve fit to model the sensors' behavior (Figure 3B). This model provides an average precision of 0.3 mm and accuracy of 0.8 mm in elongation ranges (Figure 3C).

2.4. The Cable-Driven Detrusor for the IBRoB

Considering the system requirements, we designed a cable-driven mechanism to compress the braided structure in order to correctly apply radial forces toward the internal balloon. In fact, cable actuation can provide a functional strategy to replicate detrusor function. In this way, rapid, reliable, and controlled motion can be achieved while maintaining a miniaturized structure without increasing the structure thickness. Cables arrangement and length control need to fulfill two main requirements: i) contracting the IBRoB, by guaranteeing intra-vesical pressures in a physiological range (i.e., native detrusor reaches up to maximum 6 kPa[25]) for an efficient micturition, and ii) allowing the IBRoB expansion, without hampering urine collection.

To contract the system, cables can be placed around the braided structure in one or multiple rounds and configurations. Nonetheless, to avoid increasing the detrusor rigidity and the number of cable points around the braided cylinder, we considered just three simple cases: 1-, 2-, and 3-times routing. Doing so, we experimentally measured cables' tension to choose a DC micromotor reaching the system pressure requirement. Bench tests with a linear stage revealed a 8.83 ± 0.87 N cable tension to get a minimum 3 kPa pressure at the bladder outlet (**Figure 4**A). As cable rounds will affect the time needed to reach 3 kPa pressure, the required power can be justified. We selected a 2-times routing configuration as the best match between the contraction time and the required power. Theoretical calculations using dynamic requirements resulted in a 33 mW DC micromotor to contract the system with a 2-times routing configuration.

2.5. The IBRoB Adapts to the Urine Volume

Considering the native detrusor muscles and their functionality, we developed proper control over cable's tension. The ability to implement controlled actuation is one of the most significant features of the soft bladder actuator. In this dynamic actuation, the cable's tension is adjusted in real time to avoid extra high or low radial forces on the bladder body (Movie S3, Supporting Information).

To expand the system during the filling phase, the IBRoB is programed using simple electronics and a controller which checks the cable force at the appropriate timing, see Figure 2B (e.g., every 5 min, which is enough considering the normal physiological bladder filling rates, i.e., 1.5–3 mL min^{-1}[31]). Figure 4B shows the intervals between micromotor actions and their current consumption as representatives of the motor torque. Indeed, depending on the current consumption, we derive the cable tension, and we decide

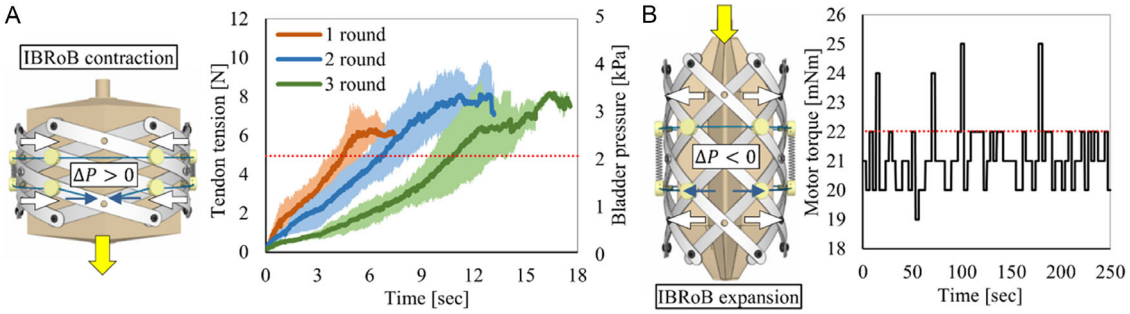

Figure 4. Cable tension in contraction and expansion phases. A) The tensions in three different routing configurations. B) The cable tension control during expansion phases.

© 2025 The Author(s). Advanced Intelligent Systems published by Wiley-VCH GmbH

26404567, 2026, 2, Downloaded from https://advanced.onlinelibrary.wiley.com/doi/10.1002/aisy.202500516 by Veronica Iacovacci - UNIVERSITY OF ESSEX , Wiley Online Library on [24/06/2026]. See the Terms and Conditions (https://onlinelibrary.wiley.com/terms-and-conditions) on Wiley Online Library for rules of use; OA articles are governed by the applicable Creative Commons License

whether to release the cable or keep it (Figure 2B). As per the calibration of the IBRoB, the cable length will be released 3 mm if the measurement results in a higher tension than 5 N or 22 mNm (equal to ≈2 kPa inner bladder pressure, see Figure 4A).

2.6. The IBRoB Estimates the Urine Volume

The IBRoB is designed to follow a predictable shape during expansion (i.e., from star shape to hexagon) since the balloon vertices are constrained in the links of the braided structure. We exploited the balloons geometric characteristics and the sensors' length to estimate the internal volume.

Considering that the bladder filling rates may vary in the human population according to the diet and lifestyle, the expansion strategy and sensing method were first tested on bench-top experiments. The expansion strategy and sensing method successfully followed a variety of constant input flow rates (see **Figure 5**B,C, and S1, Supporting Information), with an average error in the volume reconstruction of 8.4 ± 6.1 mL and a maximum 58.5 mL error. The average error was only 2.8% of the balloon's full capacity.

To verify the system in a more realistic scenario, where bladder filling rates can randomly vary,[32] we evaluated the capability of the device in a human phantom, filled with animal tissues mimicking the organs encumbrance around the bladder. Various flow rates were varied along a single filling phase (see **Figure 6**C), and the volume estimation resulted in an average error of 25.6 ± 11.9 mL and a maximum 76.4 mL error. The average error was only 6.4% of the balloon's full capacity.

2.7. The IBRoB Assists Micturition

The trials of urine volume reconstruction have ended with a voiding phase by activating the cable-based actuation mechanism. We have positioned the IBRoB horizontally (see Figure 5A and Movie S3, Supporting Information) to simulate the worst-case scenario of bedridden patients and positioned it in a sloped orientation, with an angle of 35° (see **Figure 7**A). In addition, to show the system performance, we tested the same configurations without any cable actuation, i.e., spontaneous voiding by gravity.

The results obtained with horizontally positioned IBRoB showed $96 \pm 1.3\%$ voiding of the initial volume within 200 s (see Figure 7B), with steady-state residual volume of maximum of 10 mL, equivalent to 3.3% of the balloon's full capacity. However, when the IBRoB was positioned and actuated in a sloped orientation (mixing gravity and cable voiding), we obtained 99% voiding in less than 90 s with a steady-state volume of maximum of 5 mL. This is an ideal condition of micturition, such as a patient sitting on a toilet. Both tests without any cable actuation resulted in ≈58% voiding within 4 min with a steady-state residual volume over 100 ml (33.3% of the capacity), which is considered clinically detrimental for the urinary system[23] (see Figure 7C). In the trials with a human phantom, we obtained

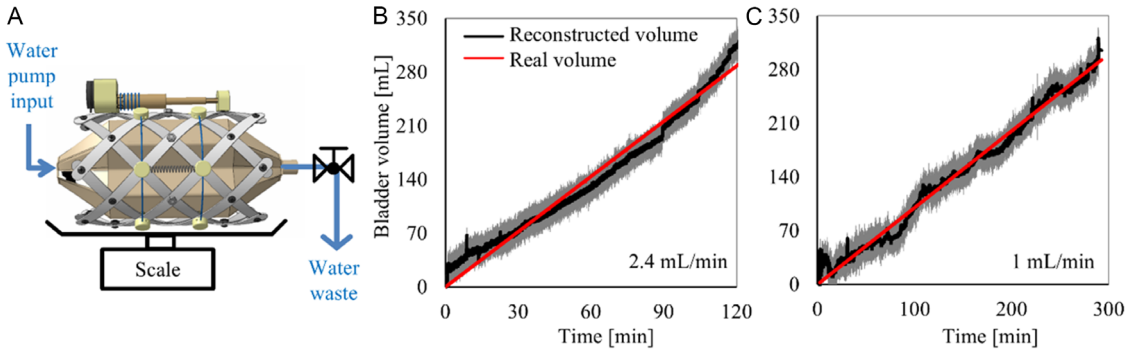

Figure 5. The system volume estimation results. A) The schematic of the experimental set-up in horizontal condition. B,C) The system performance with constant filling speed of 2.4 and 1 mL min^{-1}, respectively.

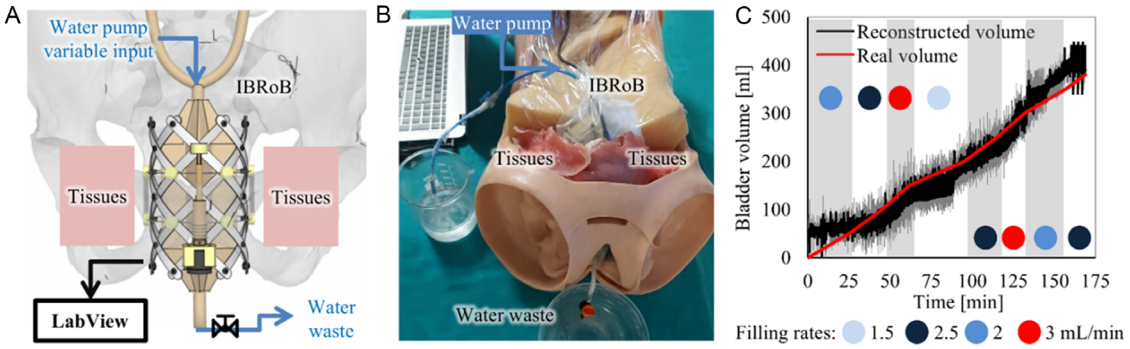

Figure 6. In vitro human phantom experiment. A) The schematic of the experiment. B) The real experimental set up. C) The system performance at various filling speeds for each 50 mL bladder volume increase.

© 2025 The Author(s). Advanced Intelligent Systems published by Wiley-VCH GmbH

26404567, 2026, 2, Downloaded from https://advanced.onlinelibrary.wiley.com/doi/10.1002/aisy.202500516 by Veronica Iacovacci - UNIVERSITY OF ESSEX , Wiley Online Library on [24/06/2026]. See the Terms and Conditions (https://onlinelibrary.wiley.com/terms-and-conditions) on Wiley Online Library for rules of use; OA articles are governed by the applicable Creative Commons License

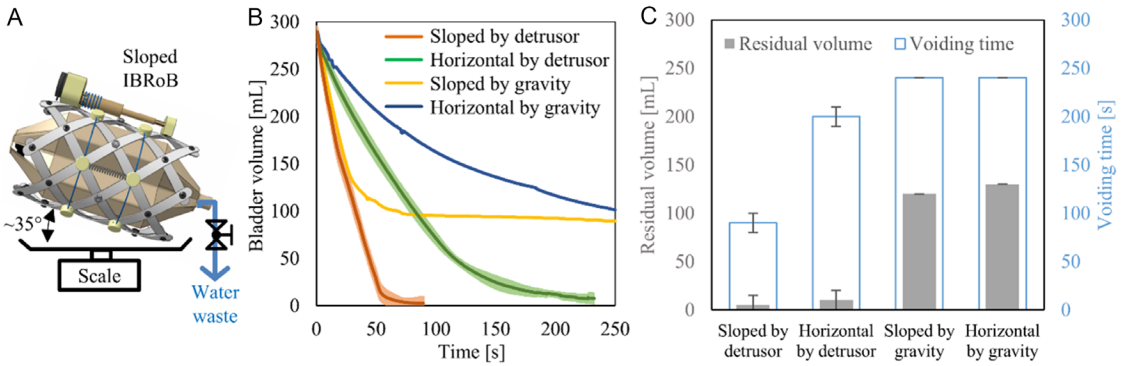

Figure 7. The system voiding results. A) The schematic of the experiment in a sloped condition. B) The system voiding performance in horizontal and sloped conditions, spontaneous gravity voiding, and when the IBRoB detrusor was actuated. C) The residual volume and the voiding time for all the conditions.

$93 \pm 1.9\%$ voiding of the initial volume within 60.4 ± 8.9 s. In this case, the bladder was placed horizontally.

3. Discussion and Conclusion

Although the urinary diversion and neobladder are a conventional clinical solution for patients who undergo radical cystectomy, they strongly affect their quality of life (e.g., the need for an external collection bag and the loss of bladder fullness sensation). In this sense, the presented IBRoB potentially offers several advantages, being a fully implantable robotic organ able to i) hold urine during the bladder filling phase; ii) expand autonomously with antireflux sphincter to avoid kidneys damages; iii) monitor the urine accumulation; and iv) compress efficiently during the voiding phase to enable the expulsion of urine with low postvoiding residual urine.

A comprehensive review of actuation principles and their challenges has been reported in the state of the art.[33] In our context, the braided structure serves to constrain radial expansion and convert a length or volume change into an uniform internal pressure, which can enhance its mechanical efficiency. Such a design approach can be integrated with fluid-based, electrothermal, or electrical actuators. Considering fabrication complexity, durability, and application-specific requirements, we selected a simple DC micromotor for the IBRoB, which is a reliable, miniature, and low-power option for implantable systems.

The IBRoB is designed with integrated electronics, both for actuation and for sensing, so that the device can only run on a 3.7 V battery in a small box. The in vitro experiments have demonstrated that the system is capable of correct functioning. In our design, the electrical boards are packed in a separate box that can stay subcutaneously inside the abdomen (Figure 2A).

The balloon and braided structure sizes were scaled in accordance with the adult human anatomy and validated on a phantom model. In this work, we prototyped and tested bladder sizes that can accommodate up to 400 mL. IBRoB in full capacity forms a diameter and height of 94 and 105 mm, respectively. Despite its large capacity, the foldable and flexible design of the entire IBRoB makes it possible to transform into a thinner cylinder-like shape with a diameter and height of 47 and 150 mm, respectively. Therefore, a surgeon can easily place it through a 50 mm wide incision through a laparoscope or robotic surgery.[17] Nonetheless, bigger or smaller sizes may be developed depending on patient-specific anatomical constraints.

We chose latex as the base material of the balloon and the sealing cover because it allowed us to easily fabricate low-cost prototype.[34] However, our design can readily be manufactured using other biocompatible materials such as certified medical-grade silicones[35] with careful consideration given to their long-term performance in the urinary environment.[36,37] Incorporating such materials, potentially combined with multilayer biocompatible coatings, will be a critical step toward enabling safe and durable long-term implantation of the proposed system. In particular, resistance to urine encrustation and biofilm formation is essential: these processes are strongly influenced by material surface properties such as roughness, porosity, and microdefects, as well as by local urine chemistry and flow dynamics.[38] While encrustation was not evaluated in this study, future work will assess material stability and encrustation resistance under physiological urinary conditions.

Considering the sensing system, the inductance sensing solution presented in IBRoB can be reliable and precise if properly isolated from the surrounding environment. This effect is more pronounced in the presence of biological tissue, where nearby structures can introduce additional interference. This was also reflected in our human phantom experiments, which showed a slightly higher error and standard deviation in the measurements. To address this, a separate calibration phase after implantation may be required, or alternatively, advanced modeling and learning-based methods could be employed to ensure long-term adaptation.

The system using the dynamic actuation principle showed very low average error in following both constant and variable urine flow rates during bladder filling, even in the presence of surrounding tissues. Dynamic actuation is a key feature of IBRoB to avoid unintended expansions of the bladder due to its structural elasticity. An analysis of the performance without dynamic expansion (i.e., releasing completely after micturition) has been presented in Figure S2, Supporting Information. As shown in the analysis, friction between links would prevent smooth expansion, leading to a stop and sudden expansion,

© 2025 The Author(s). Advanced Intelligent Systems published by Wiley-VCH GmbH

26404567, 2026, 2, Downloaded from https://advanced.onlinelibrary.wiley.com/doi/10.1002/aisy.202500516 by Veronica Iacovacci - UNIVERSITY OF ESSEX , Wiley Online Library on [24/06/2026]. See the Terms and Conditions (https://onlinelibrary.wiley.com/terms-and-conditions) on Wiley Online Library for rules of use; OA articles are governed by the applicable Creative Commons License

26404567, 2026, 2, Downloaded from https://advanced.onlinelibrary.wiley.com/doi/10.1002/aisy.202500516 by Veronica Iacovacci - UNIVERSITY OF ESSEX , Wiley Online Library on [24/06/2026]. See the Terms and Conditions (https://onlinelibrary.wiley.com/terms-and-conditions) on Wiley Online Library for rules of use; OA articles are governed by the applicable Creative Commons License

resulting in inaccurate volume reconstruction and high negative pressure in the bladder and, subsequently, in the ureters. In fact, high negative pressures can disturb renal function and potentially lead to obstruction of the renal pelvis over time.[39]

The IBRoB represents a step forward in the field of implantable robotics devices for patients who undergo radical cystectomy. Although the systems previously presented in state-of-the-art employing magnetic actuation[17] reported adequate performances (i.e., reaching 4 kPa pressure), their passive operation would produce high intra-vesical negative pressure. On the other hand, using shape memory alloy wires for the detrusor consumes a substantial amount of current and rapidly reaches a temperature above 80°.[40] The sensing solution based on capacitive sensors[13] cannot be integrated with implantable devices due to their bulky measurement electronics.[14]

The proper functioning of the current IBRoB requires a power budget of only 46.3 mAh, which could be decreased by optimizing the control scheme.[41] Future developments can easily embed an implantable battery, which can be recharged using wireless charging principles as described in a previous work.[42,43]

The current prototype has successfully performed around 65 voiding cycles without degradation in its performance, which is sufficient for a short-term in vivo implantation trial. While the DC motor itself has a long lifetime, precise fabrication and robust materials can even extend the system reliability for longer trials.

Transitioning this system toward in vivo studies introduces several important challenges, including immune response, tissue integration, and long-term mechanical stability. Chronic implantation requires materials that are biocompatible, compliant, and resistant to local irritation, fibrosis, and encrustation, while interfaces with the ureters and bladder must maintain leak-proof connections under physiological urine flow. In addition, the device must sustain repeated filling and voiding cycles without loss of function or structural integrity.

At this stage, we used mechanical valves as a urinary sphincter in filling phases. However, in future development stages toward in vivo implantation, electromagnetic valves can be integrated. Another still open engineering challenge of the IBRoB is the configurable sealing of the device to avoid the contact of the electronics and the aggressive body fluids, due to large expansion-contraction-expansion motions of the balloon.

Addressing these challenges will involve careful material selection, interface optimization, and staged preclinical evaluation, starting with acute implantation studies to assess surgical implant procedure, short-term device operation, and body response to the implant.[44] These observations will be considered as high priorities to move toward a long-term in vivo implantation in large animal models.

4. Experimental Section

Fabrication of the Ureter Antireflux Valve: The antireflux valve is placed on the top section of the balloon, where it connects to the kidneys through the ureters. Fabrication was carried out by pouring prevulcanized liquid latex onto a flat smooth surface and passing a film spreader, which was set to 0.5 mm layer thickness (**Figure 8**A). The film was cured for one hour at room temperature and humidity. Next, the film was peeled off, and two semicircular shapes were cut with a laser cutting machine. A sacrificial paper substrate was placed onto the lower layer of latex, and extra latex was brushed over the entire surface, including the edges. Then, firstly, a top layer of latex was placed, and secondly, a weight was placed over the whole sample sandwich. The sample was cured for two hours at room temperature and humidity. The paper was removed by water wetting and pushing it off with high air pressure.

Preparation of the Hexagon Balloon and Characterization of the Ureters Valve: The hexagon balloon was fabricated through a dip molding process of latex polymer, resulting in a thin and soft body (about 4 mm thick). The balloon size was determined using anatomical constraints in human body and native bladder full capacity (i.e., 300–400 mL (30)). The fabrication process was carried out in the following steps (Figure 8A): i) CAD design; ii) 3D printing the hexagon core mold; iii) twice dipping of the 3D-printed core into an uncured latex container followed by air curing (≈4 h); vi) removal of the internal mold by making a cut, subsequently closed with additional latex pouring; v) positioning of semirigid acetate components (obtained by laser cutting technique) with bio-adhesive double-sided tape on side walls as reinforcement; vi) twice dipping into an uncured latex container followed by air curing (≈4 h). Ureters are then manually stitched to the latex bladder prototypes. In this way, different dimensions can be easily scaled to conform to different anatomies.

In order to characterize the ureter antireflux valve, three bladder samples, each with one ureter, were fabricated. The prototypes were positioned horizontally on a support surface, while the side with the ureter was placed above a scale to collect any leaking drops (Figure 8B). On the other free side, the balloon was connected to a pressure sensor (NXP semiconductors MPXV5010DP, The Netherlands), transmitting data to an Arduino Due, serially connected to a laptop. The set up allowed to measure the pressure leading to leakage in the valve. A set of loads (i.e., 0, 8.3, 19.1, and 23.5 N) was placed on the upper surface of the balloon for 60 s, and the results of all samples were averaged.

Preparation of the Flexible Braided Links: The links were obtained using 1 mm-thick PETG sheet (RS Pro, Italy) and a laser cutting machine. PETG is FDA approved and has the best shear strength, durability, and flexibility for the expected mechanical functionality of the braided structure (i.e., 50% elongation before breaking and 2150 MPa Flexural Modulus). Our design followed a scissor linkage mechanism in which the links were bent into a cylinder shape and held together with bolted joints (**Figure 9**A). Considering a simple scissor mechanism involving 4 links, each cross will remain on one half of the shape. Thus, the link length was determined based on the half hexagon circumference. Due to the fact that the braided link will need to be attached to the hexagonal balloon, we considered 12 links for shaping the braided link structure (Figure 9A). Then, for attaching the braided structure to the latex balloon, six plastic screws were glued to the middle of balloon vertices. As a final step, at each intersection of the link pairs, a loose M3 bolted joint provides link attachments and custom eyelets for securing actuation cables.

Sensing Design and Characterization: Inductance sensors were chosen among the smallest tension springs that were commercially available. In addition, since the spring causes a resistance to contraction of the system, a low spring constant was considered in choosing the sensor. A pair of steel springs with an outer diameter of 1.15 mm and a stiffness of 0.05 N mm^{-1} was sized in 10 mm initial length, and tied to the cable eyelets. We experimentally measured the inductance changes while the springs were in cyclic elongations. The experimental set up is illustrated in Figure 9B and Movie S2, Supporting Information, in which a linear stage actuator (M414, PI, USA) elongates the braided structure. In the first experiment, we elongated the sensor from 12.5 to 32.5 mm at three different speeds (i.e., 1, 2.5, and 5 mm sec^{-1}), considering a possible fast or slow expansion. Each speed was repeated 5 times, and the averaged results are shown in Figure 3B. We have fitted an exponential curve to the results and used the acquired formula for estimating the spring length. In the second experiment, we investigated the accuracy (averaged error) and precision (averaged deviation) of the sensors at various target points using the acquired formula, as shown in Figure 3C.

IBRoB Design and Geometrical Model for Volume Estimation: The balloon design is composed of a core prism with hexagonal base and two pyramids on the top and on the bottom of the prism (see **Figure 10**A). In its expanded configuration of 400 mL balloon, the hexagon sides are equal

© 2025 The Author(s). Advanced Intelligent Systems published by Wiley-VCH GmbH

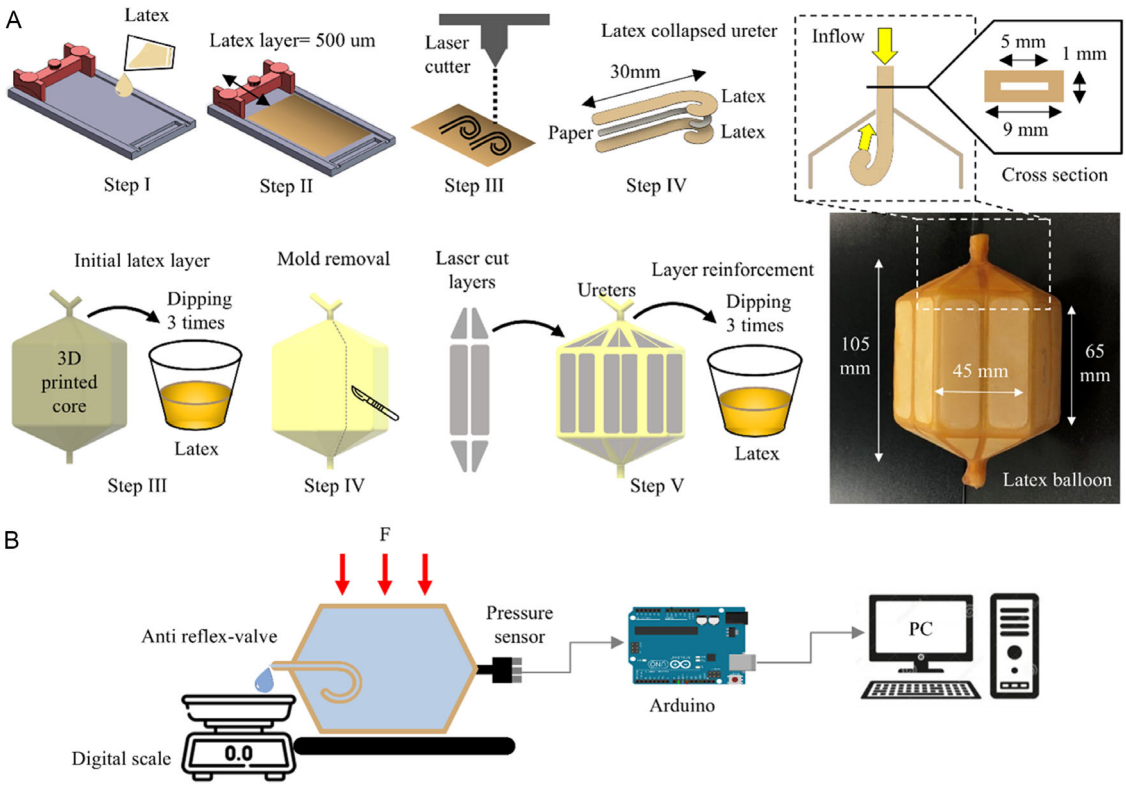

Figure 8. A) Fabrication steps of the antireflux ureters and bladder in the first and second row, respectively. B) Setup to verify the absence of backflow during compression.

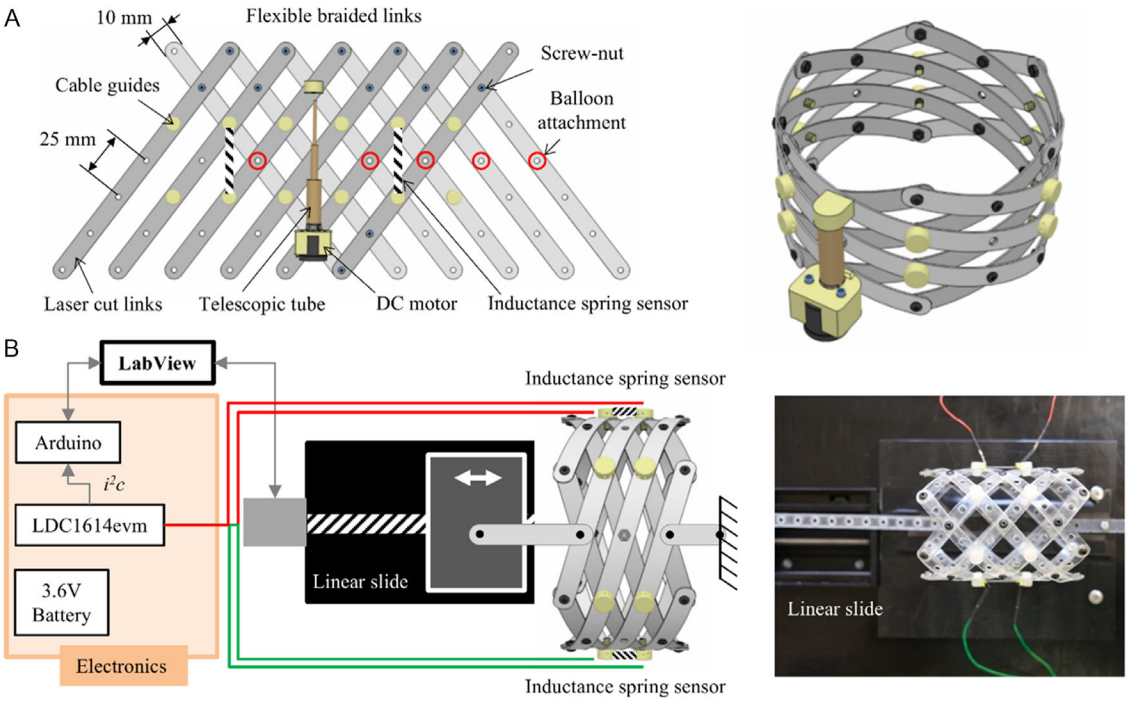

Figure 9. A) Linkages assembly, actuation, and sensing assembly to realize the braided structure. B) Set up to evaluate inductance sensors' performance. One side is fixed with a small linkage, whereas the opposite extremity is pulled by a linear sliding system, controlled with a LabView interface.

© 2025 The Author(s). Advanced Intelligent Systems published by Wiley-VCH GmbH

26404567, 2026, 2, Downloaded from https://advanced.onlinelibrary.wiley.com/doi/10.1002/aisy.202500516 by Veronica Iacovacci - UNIVERSITY OF ESSEX , Wiley Online Library on [24/06/2026]. See the Terms and Conditions (https://onlinelibrary.wiley.com/terms-and-conditions) on Wiley Online Library for rules of use; OA articles are governed by the applicable Creative Commons License

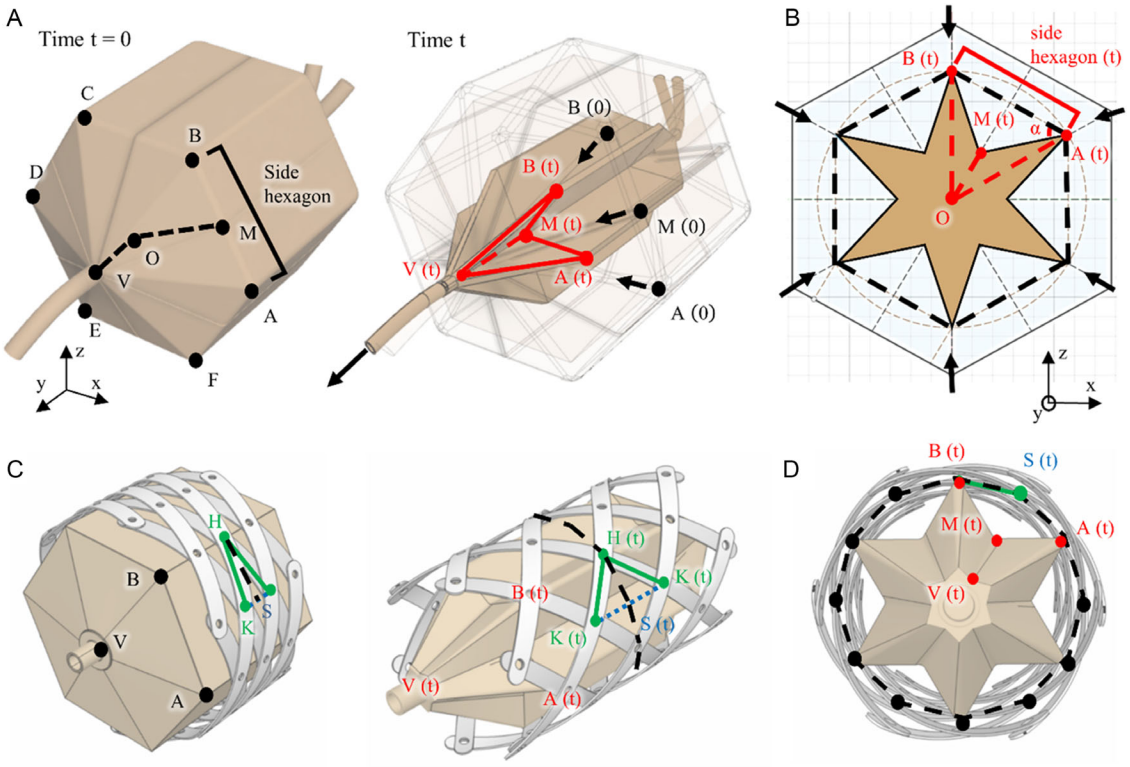

Figure 10. A) Filled and collapsed configurations of the hexagon balloon models in 3D view. B) Side view of the hexagon balloon. C) IBRoB design and geometrical model in filled and collapsed configurations. D) Side view of the IBRoB model.

to 45 mm, while the core prism and overall height are 65 and 105 mm, respectively. When collapsed, its height reaches 155 mm. Regarding the outer braided structure, the system was designed with dimensions able to fit the expanded hexagon balloon, which is a cylindrical shape with 94 mm in diameter and 105 mm in height. Whereas in its collapsed configuration, it reaches 47 mm in diameter and 150 mm in height.

The overall bladder volume can be estimated by knowing the indentation's position in time of the star shape, $\overline{OM}(t)$, and the height of the pyramids, $\overline{OV}(t)$ (Figure 10). To do so, the following considerations must be taken into account: that is, given $\widehat{BAM}(t) = \alpha(t)$, with $0 \leq \alpha(t) \leq \pi/3$, and M as middle point of $\overline{AB}(0)$.

By its design, we know at a generic time instant t_1

$$\forall t\, \overline{AM(t_1)} = \overline{MB(t_1)} = \frac{\text{side}_{\text{hexagon}}}{2} = 22.5\,\text{mm} \tag{1}$$

$$\forall t\, \overline{BV(t_1)} = \sqrt{\overline{OB}^2(0) + \overline{OV}^2(0)} \approx 49\text{mm} \tag{2}$$

$$\forall t\, R(t_1) = \overline{OA}(t_1) (\equiv \overline{OB}(t_1) \equiv \overline{AB}(t_1)) \tag{3}$$

hence, at time instant $t = 0$, we have that: $\overline{OA}(0) = R(0) = 45$ mm. Assuming to have a symmetrical collapsing system, thanks to the braided structure, at a generic time instant t, the star section of Figure 10B,C is inscribed in a theoretical hexagon of side length $R(t)$. Thus

$$\begin{aligned} R(t_1) &= \overline{OA}(t_1) = 2(\overline{AM(t_1)})\cos(\alpha(t_1)) \\ &= 2\left(\frac{R(0)}{2}\right)\cos(\alpha(t_1))(\equiv \overline{OB}(t_1) \equiv \overline{AB}(t_1)) \end{aligned} \tag{4}$$

$R(t)$ and $\alpha(t)$ can be estimated by means of the spring sensor and the geometry of the braided structure. As depicted in Figure 10D, by design, we have the following conditions

$$\forall t\, \overline{KH(t_1)} = l_{\text{linkage}} = 25\,\text{mm} \tag{5}$$

$$\forall t\, \overline{KS(t_1)} = l_{\text{sensor}}(t_1)/2 \tag{6}$$

Being the structure a cylindrical shape, we can consider the Pythagorean theorem valid, so we have the following condition, where

$$\overline{HS(t_1)} = \sqrt{{l_{\text{linkage}}}^2 - \frac{{l_{\text{sensor}}(t_1)}^2}{4}} \tag{7}$$

$\overline{HS(t_1)}$ is a side of the theoretical dodecagon that can be described around the model (Figure 10D). So

$$R(t_1) = \overline{HS(t_1)} \times \frac{2}{(\sqrt{6} - \sqrt{2})} \tag{8}$$

from this, we inversely estimate $\alpha(t_1)$, as

$$\alpha(t_1) = \cos^{-1}\frac{R(t_1)}{R(0)} \tag{9}$$

knowing these values, it is possible to estimate the needed parameters

$$\begin{aligned} \overline{OM}(t_1) &= h_{\Delta OBA(t_1)} - h_{\Delta MBA(t_1)} = \overline{OA}(t_1)\sin\left(\frac{pi}{3}\right) \\ &- \left(\frac{R(0)}{2}\right)\sin(\alpha(t_1)) = R(0) \\ &\times \left(\frac{\sqrt{3}}{2}\cos(\alpha(t_1)) - \left(\frac{\sin(\alpha(t_1))}{2}\right)\right) \end{aligned} \tag{10}$$

© 2025 The Author(s). Advanced Intelligent Systems published by Wiley-VCH GmbH

26404567, 2026, 2, Downloaded from https://advanced.onlinelibrary.wiley.com/doi/10.1002/aisy.202500516 by Veronica Iacovacci - UNIVERSITY OF ESSEX , Wiley Online Library on [24/06/2026]. See the Terms and Conditions (https://onlinelibrary.wiley.com/terms-and-conditions) on Wiley Online Library for rules of use; OA articles are governed by the applicable Creative Commons License

$$\overline{OV}(t_1) = \sqrt{\overline{BV}^2 - \overline{OB}^2(t_1)} = \sqrt{49^2 - R^2(t_1)} \tag{11}$$

From these parameters, the volume can be estimated as a composition of the two pyramids and core prism, at any generic instant, as

$$\text{Volume}(t_1) = \nu_{\text{prisma}(t_1)} + 2 \times (\nu_{\text{piramide}(t_1)}) \tag{12}$$

$$\begin{aligned}\text{Volume}(t_1) = 65 \times \Bigg(& \left(\frac{3\times\sqrt{3}}{2}\right) \times \left(R(0) \times \sin^2\left(\frac{\text{pi}}{3} - \alpha(t_1)\right)\right) \\ & + 6 \times \left(\frac{R(0)^2}{4} \times \sin\left(\frac{\text{pi}}{3} - \alpha(t_1)\right) \times \cos\left(\frac{\text{pi}}{3} - \alpha(t_1)\right)\right)\Bigg) \\ & + \frac{\sqrt{49^2 - R^2(t_1)}}{3} \times \left(\frac{3\times\sqrt{3}}{2}\right) \times \left(R(0) \times \sin^2\left(\frac{\text{pi}}{3} - \alpha(t_1)\right)\right. \\ & \left. + \left(\frac{R(0)^2}{2} \times \sin\left(\frac{\text{pi}}{3} - \alpha(t_1)\right) \times \cos\left(\frac{\text{pi}}{3} - \alpha(t_1)\right)\right)\right)\end{aligned} \tag{13}$$

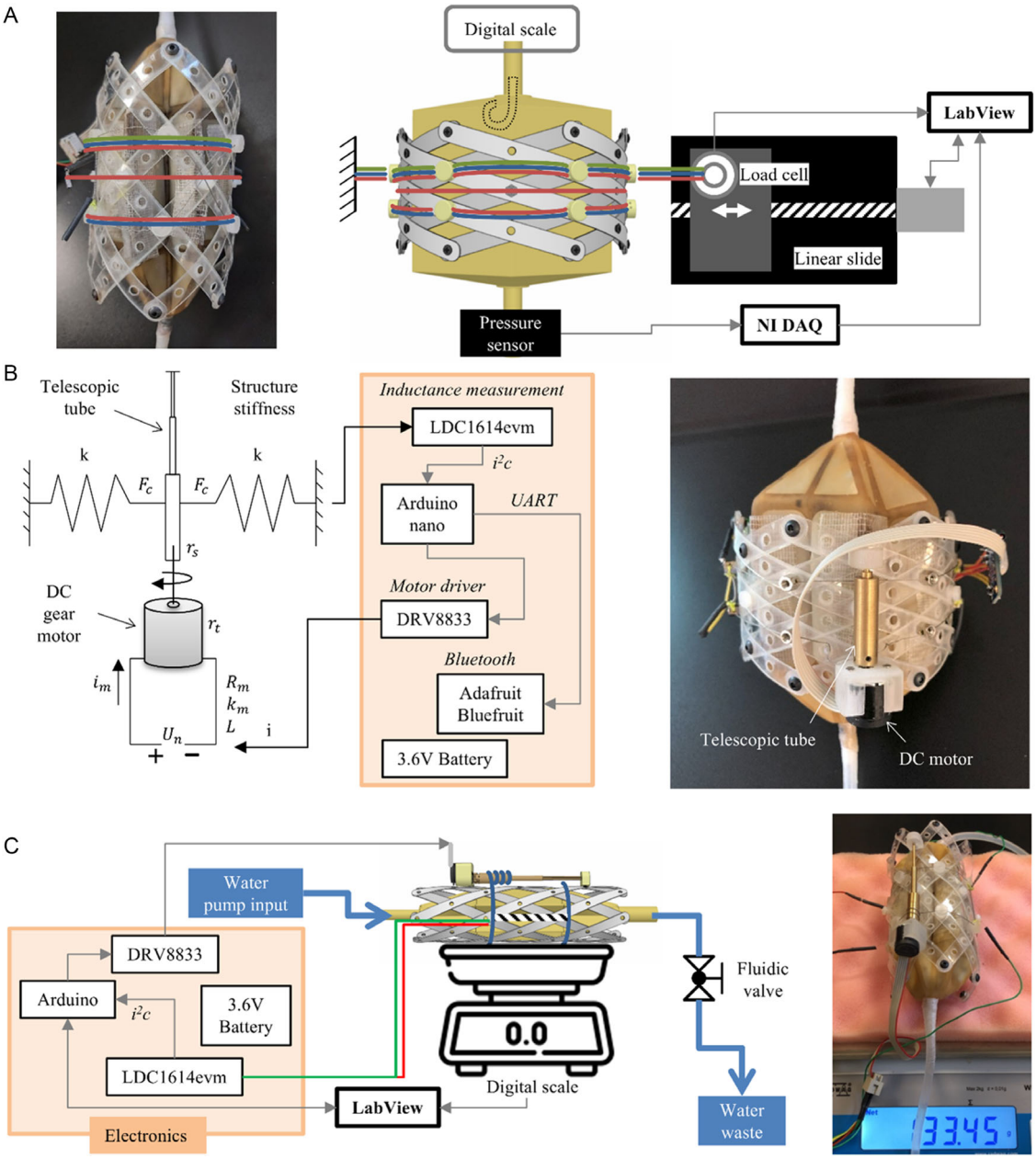

Figure 11. A) Set up to evaluate the cable actuation mechanism. One side of the cables is fixed, whereas the other side is linked to a load cell. B) The ideal mechanical and electrical model of the IBRoB. C) Set up to verify the IBRoB efficiency in reconstructing volume during filling phase and voiding performance.

© 2025 The Author(s). Advanced Intelligent Systems published by Wiley-VCH GmbH

26404567, 2026, 2, Downloaded from https://advanced.onlinelibrary.wiley.com/doi/10.1002/aisy.202500516 by Veronica Iacovacci - UNIVERSITY OF ESSEX , Wiley Online Library on [24/06/2026]. See the Terms and Conditions (https://onlinelibrary.wiley.com/terms-and-conditions) on Wiley Online Library for rules of use; OA articles are governed by the applicable Creative Commons License

Actuation Design and Calibration: A motor actuator was selected based on the required force and speed to collapse the braided link structure. In addition, size, operating voltage, and simplicity of driving electronics were also considered as requirements in the design of implantable robotic devices. We experimentally measured the cable tension in three possible routing configurations to estimate the required DC motor torque. The experimental set up is shown in **Figure 11**A, in which a linear stage actuator pulls the cable at constant speed. One side of the cable was fixed to the baseplate, and the other side was fixed to a load cell (ATI nano17, USA) on the moving plate. This experiment was initiated with a full IBRoB and terminated once the output pressure reached 3 kPa. The experiment was repeated five times for each cable routing, and the averaged results are shown in Figure 4A.

In order to design the actuation system, a small 3D printed holder was used to fix the DC motor (Faulhaber 1512U003SR 324:1) and the braided link. Motor's shaft was attached to a telescopic tube with three segments. The one connected to the motor has the largest diameter (i.e., 8 mm), while the one attached to the braided link has the smallest diameter (i.e., 2 mm). The telescopic tube has a running clearance fit, and its length can change from 25 to 65 mm. The actuation cables were tied to the big tube through two holes.

We calibrated the cable release strategy by taking into account the motor current constant (equal to 0.48 A mNm^{-1}), the largest diameter of the telescopic tube, and the tension necessary to achieve a pressure of 2 kPa in the bladder. It was necessary to perform this calibration step in order to adjust the threshold value without having to estimate the friction between the cable and eyelets. The results are shown in Figure 4B.

IBRoB Actuation Model: Motor and gearhead selection was done on the basis of an ideal physical model, as in Figure 11B. To simplify modeling, the mechanical properties of the links and balloon are assumed to be linear elastic; as such, they can be modeled as a spring with stiffness k. The DC motor is modeled using two opposing voltage sources and a resistor. One voltage source for the motor supply voltage, one source for the motor back-EMF, and a resistor for the motor terminal resistance R_m. The gearhead is represented by transmission ratio r_t (rotation to rotation) and efficiency η_t. The telescopic tube is represented by radius r_s (motor rotation to cable translation) and efficiency η_s. Lastly, the cable guide eyelets are represented with efficiency η_p.

The required cable force F_c and cable velocity v_c are known from the dynamic requirements and experimental data on the system (10 N, within 3 s, over 0.01 m range). A second-order displacement function is used to define position and velocity behavior over time. Consequently, the cable force is defined by a second-order function as well. Using the cable force, the required motor torque M can be calculated as follows

$$M = 2F_c \frac{r_s}{r_t} \frac{1}{\eta_t \eta_s \eta_p} + i_{nl} k_m \tag{14}$$

The last term represents the motor frictional torque, which can be calculated using the motor torque constant k_m and the motor no-load current i_{nl}. The motor velocity ω_m can be calculated as follows

$$\omega_m = v_c \frac{r_t}{2r_s} \tag{15}$$

therefore, for a low inductance motor, the motor voltage u_m and motor current i_m can be calculated using

$$i_m = \frac{M}{k_m} \tag{16}$$

$$u = i_m R_m + \omega_m k_m \tag{17}$$

The motor power balance can be used to calculate the motor mechanical power P_{mech}, motor electrical input power P_{elec}, motor copper losses P_j, and motor efficiency η_m over time

$$P_{\text{elec}} = P_{\text{mech}} + P_j \tag{18}$$

$$u_m i_m = (M - i_{nl} k_m)\omega_m + i_m^2 R_m \tag{19}$$

$$\eta_m = \frac{P_{\text{mech}}}{P_{\text{elec}}} = 1 - \frac{P_j}{P_{\text{elec}}} = \frac{(M - i_{nl} k_m)\omega_m}{u_m i_m} \tag{20}$$

The system efficiency η_{sys} (efficiency of the complete actuation unit) can be calculated by multiplying the motor efficiency η_m by the transmission efficiency (η_t, η_p, η_s). Therefore, it is a scaled version of the motor efficiency η_m and relates the electrical input power P_{elec} to the output power (**Table 1**) (multiplication of cable force and cable velocity).

$$\eta_{\text{sys}} = \eta_m \eta_t \eta_p \eta_s = \frac{F_c v_c}{u_m i_m} \tag{21}$$

IBRoB Electronics: In order to design the system suitable for in-body implantation, the motor was connected to a miniature driver board (Adafruit, DRV8833, USA) and ultimately to a controller board (Arduino nano, Italy). We measured the current passing through the motor by placing a 1 Ω sense resistor in series with the motor. The springs were connected to an inductance measurement board (LDC1614evm, TI, USA) and i^{2}c communication to the Arduino. The sensors were sampled at 100 Hz, then each 10 samples were averaged and transferred to the serial port. As part of the benchtop experiments, we used a USB communication link with LabView 2020 software; anyhow, a Bluetooth module (e.g., Adafruit Bluefruit LE UART) can be used. The presented electronics can work with a 3.7 V rechargeable Li-Ion battery such as Resonetic Contego 440 (capacity of 440 mAh and dimensions of 23 × 38 × 7 mm).

IBRoB Power Budget: In order to estimate the overall power consumption of IBRoB, average activation periods were considered based on the workflow presented below:

In the sensing-volume estimation loop, first the cable tensioning loop is checking the tensions, and then the sensors read-out will reconstruct the urine volume at 5-min intervals and exchanges data with the app for 5 s (5 min: 295 s in sleep mode, and 5 s active). Considering the daily volumetric urine output (maximum 2000 mL day^{-1}), the cable releasing mechanism can work up to 25 min per day. Assuming 80% capacity of IBRoB, and voiding duration (4 min); the voiding mechanism can work up to 28 min per day.

According to the data sheets of all the components, the estimated power consumption of the device is summarized in **Table 2**. Based on that,

Table 1. Characteristics of the DC gear motor: Faulhaber 1512U003SR 324:1.

Values at 22° and nominal voltage		Value
Nominal voltage	U_N	3 V
Terminal resistance	R_m	10.4 Ω
Efficiency, max	η_t	53%
No-load speed	n_0	15 min^{-1}
No-load current	i_{nl}	0.01 A
Stall torque	M_H	50 mNm
Speed constant	k_n	4640 min^{-1}/V
Back-EMF constant	k_E	0.216 mV/min^{-1}
Torque constant	k_M	2.06 mNm/A^{-1}
Current constant	k_I	0.486 A/mNm^{-1}
Slope of n-M curve	$\Delta n/\Delta M$	24 700 min^{-1}/mNm
Rotor inductance	L	175 µH
Mechanical time constant	τ_m	17 ms
Rotor inertia	J	0.09 gcm^2
Angular acceleration	$\alpha_{max.}$	68·10^{3}rad/s^2

© 2025 The Author(s). Advanced Intelligent Systems published by Wiley-VCH GmbH

26404567, 2026, 2, Downloaded from https://advanced.onlinelibrary.wiley.com/doi/10.1002/aisy.202500516 by Veronica Iacovacci - UNIVERSITY OF ESSEX , Wiley Online Library on [24/06/2026]. See the Terms and Conditions (https://onlinelibrary.wiley.com/terms-and-conditions) on Wiley Online Library for rules of use; OA articles are governed by the applicable Creative Commons License

Table 2. Estimated power consumption of IBRoB.

	Current [mA]	Time [s day^{-1}]	Current × time [mAs day^{-1}]
Cable releasing	1	1500	1500
Cable tensioning, sensing, and communication	50	1440	72 000
Voiding, sensing, and communication	55	1680	92 400
Sleep mode	0.01	81 780	817
Total			166 717

the IBRoB is expected to need 46.3 mAh per day. Considering the battery capacity, IBRoB guarantees 9 days of working without needs of a charging cycle.

Bench Top Experiments on Bladder Volume Estimation: We experimentally evaluated the performance of volume estimation and size expansion when the system was supplied with a constant flow rate. Bench top test set up is shown in Figure 11C. An assembled prototype was placed on a digital precision balance (RADWAG, WLC 2/A2, Poland) with USB data output at 10 Hz. The prototype's outlet was connected to a fluid electronic valve and ultimately to a water waste container. The prototype's inlet was connected to a syringe pump (NE-1010, KF Technology, Italy) with variable flow rate control. The trials were initiated in an empty state; when it reached its full state, the outlet valve was opened, and the actuation cable pushed water out (Movie S3, Supporting Information). There were five repetitions of each trial using constant flow rates (1, 2.4, 5, 10 mL min^{-1}). These flow rates were considered, looking at urine production rate in healthy humans.[32] The results are shown in Figure 5 and S1, Supporting Information.

In Human Phantom Experiment: In the next experimental phase, we evaluated the IBRoB performance in a human phantom model. This benchtop test set up is shown in Figure 6A,B. The assembled prototype and its electronic components were wrapped in a sealing cover to simulate the protection of the electronic components from the body fluids and placed inside the phantom pelvic. The human mannequin was placed horizontally to test the worst voiding scenario of bedridden patient. We used some fresh animal tissues around the prototype to simulate the encumbrance of organs surrounding the bladder and to evaluate the performance in a more realistic environment. In these experiments, we used a similar methodology of bench-top volume estimation experiments, but the variable inlet flow rate was changed in 50 mL sequence from 0 to 400 mL (i.e., 2, 2.5, 3, 1.5, 2.5, 3, 2, 2.5 mL min^{-1}). Flow rates were selected based on physiological urine flow rates (i.e., 1.5 to 3 mL min^{-1}[31]). This experiment was repeated three times with the same filling sequence.

Supporting Information

Supporting Information is available from the Wiley Online Library or from the author.

Acknowledgements

The authors thank Dr. Simona Castellano for her relevant input about urinary system physiology. This work was supported by INAIL (Istituto nazionale Assicurazione Infortuni sul Lavoro), the Italian National Institute for Insurance against Work-related Injuries (noncommercial entity), within the PR19-CR-P2 BioSUP (BIOnic Solutions for Urinary impaired People) project framework, and by FIS (Fondo Italiano per la Scienza) project IBRIS funded by the Italian Ministry of University. The authors acknowledge the support of the BRIEF "Biorobotics Research and Innovation Engineering Facilities" (project identification code IR0000036), project funded under the National Recovery and Resilience Plan (NRRP), Mission 4 Component 2 Investment 3.1 of Italian Ministry of University and Research, funded by the European Union–NextGenerationEU.

Conflict of Interest

The authors declare no conflict of interest.

Data Availability Statement

The data that support the findings of this study are available from the corresponding author upon reasonable request.

Keywords

artificial organs, impaired urinary bladder, implantable devices, inductance sensing, robotic detrusor

Received: May 9, 2025
Revised: August 30, 2025
Published online: October 17, 2025

[1] A. Menciassi and V. Iacovacci, "Implantable Biorobotic Organs," *APL Bioengineering 4* (**2020**): 040402.
[2] M. Mehrali, S. Bagherifard, M. Akbari, et al., "Blending Electronics with the Human Body: A Pathway toward a Cybernetic Future," *Advanced Science 5* (**2018**): 1700931.
[3] Sobot, R. "Implantable Technology: History, Controversies, and Social Implications [Commentary]," *IEEE Technology and Society Magazine 37* (**2018**): 35.
[4] S. Micera, A. Menciassi, L. Cianferotti, E. Gruppioni, and V. Lionetti, "Organ Neuroprosthetics: Connecting Transplanted and Artificial Organs with the Nervous System," *Advanced Healthcare Materials 24* (**2024**): 2302896.
[5] M. Cosentino, J. M. Gaya, A. Breda, J. Palou, and H. Villavicencio "Alloplastic bladder substitution: Are we making progress?" *International Urology and Nephrology 44* (**2012**): 1295.
[6] D. M. Barrett, D. C. O'sullivan, B. G. Parulkar, M. G. Donovan, "Artificial Bladder Replacement: A New Design Concept," *Mayo Clinic Proceedings 67* (**1992**): 125.
[7] A. Atala, "Tissue engineering of human bladder," *British Medical Bulletin 97* (**2011**): 81, https://doi.org/10.1093/bmb/ldr003.
[8] Á. Serrano-Aroca, C. D. Vera-Donoso, V. Moreno-Manzano, "Bioengineering Approaches for Bladder Regeneration," *International Journal of Molecular Sciences 19* (**2018**): 1796.
[9] A. D. Mickle, S. M. Won, K. N. Noh, et al., "A wireless closed-loop system for optogenetic peripheral neuromodulation." *Nature 565* (**2019**): 361.
[10] B. Provost, and M. Sawan, "Proposed new bladder volume monitoring device based on impedance measurement," *Medical & Biological Engineering & Computing 35* (**1997**): 691, https://doi.org/10.1007/BF02510979.
[11] M. Kim, S. Lee, I. Yoon, et al. "Polypyrrole/Agarose Hydrogel-Based Bladder Volume Sensor with a Resistor Ladder Structure." *Sensors 18* (**2018**): 2288.
[12] S. Pane, T. Mazzocchi, V. Iacovacci, L. Ricotti, and A. Menciassi "Smart implantable artificial bladder: An integrated design for organ replacement," *IEEE Transactions on Biomedical Engineering 68* (**2021**): 2088.

© 2025 The Author(s). Advanced Intelligent Systems published by Wiley-VCH GmbH

26404567, 2026, 2, Downloaded from https://advanced.onlinelibrary.wiley.com/doi/10.1002/aisy.202500516 by Veronica Iacovacci - UNIVERSITY OF ESSEX , Wiley Online Library on [24/06/2026]. See the Terms and Conditions (https://onlinelibrary.wiley.com/terms-and-conditions) on Wiley Online Library for rules of use; OA articles are governed by the applicable Creative Commons License

[13] F. Arab Hassani, H. Jin, T. Yokota, T. Someya, and N. V. Thakor, "Soft sensors for a sensing-actuation system with high bladder voiding efficiency," *Science Advances 6* (**2020**): eaba0412.

[14] F. Semproni, V. Iacovacci, and A. Menciassi, "Bladder Monitoring Systems: State of The Art and Future Perspectives," *IEEE Access 10* (**2022**): 125626.

[15] X. Yang, C. An, S. Liu, et al., "Soft Artificial Bladder Detrusor," *Advanced Healthcare Materials 7* (**2018**): 1701014.

[16] F. A. Hassani, W. Y. Peh, G. G. Gammad, et al., "A 3D Printed Implantable Device for Voiding the Bladder Using Shape Memory Alloy (SMA) Actuators," *Advanced Science 4* (**2017**): 1700143.

[17] Y. Yang, J. Wang, L. Wang, et al. "Magnetic soft robotic bladder for assisted urination," *Science Advances 8* (**2022**), https://doi.org/10.1126/sciadv.abq1456.

[18] G. Casagrande, M. Ibrahimi, F. Semproni, V. Iacovacci, and A. Menciassi, "Hydraulic Detrusor for Artificial Bladder Active Voiding," *Soft Robotics 10* (**2022**): 269.

[19] S. Xiao, K. Holmes-Martin, L. Zhu, A. Pirrera, and F. A. Arab Hassani, "A Bistable Assistive Device for Wireless Control of a Dysfunctional Bladder Under Minimal Stress," *Advanced Materials Technologies 10* (**2025**): 2500253, https://doi.org/10.1002/admt.202500253.

[20] R. K. Lee, H. Abol-Enein, W. Artibani, et al., "Urinary diversion after radical cystectomy for bladder cancer: options, patient selection, and outcomes," *BJU International 113* (**2014**): 11, https://doi.org/10.1111/bju.12121.

[21] K. C. DeGeorge, H. R. Holt, and S. C. Hodges, "Bladder Cancer: Diagnosis and Treatment," *American Family Physician 96* (**2017**): 507.

[22] A. Richters, K. K. Anke, and L. A. Kiemeney, "The global burden of urinary bladder cancer: an update," *World Journal of Urology 38* (**2020**): 1895.

[23] M. H. Ho and N. N. Bhatia, "Lower Urinary Tract Disorders in Postmenopausal Women," in *Treatment of the Postmenopausal Woman*, (Elsevier, **2007**), pp. 693–737.

[24] G. Williams, J. T. Fletcher, S. I. Alexander, and J. C. Craig, "Vesicoureteral Reflux," *Journal of the American Society of Nephrology 19* (**2008**): 847.

[25] R. T. Kershen, K. M. Azadzoi, and M. B. Siroky, "Blood Flow, Pressure and Compliance in the Male Human Bladder," *Journal of Urology 168* (**2002**): 121.

[26] Y. Aoki, H. W. Brown, L. Brubaker, J. N. Cornu, J. O. Daly, and R. Cartwright, "Urinary incontinence in women," *Nature Reviews Disease Primers 3* (**2017**): 1.

[27] R. Viana, E. Batourina, H. Huang, et al., "The development of the bladder trigone, the center of the anti-reflux mechanism," *Development 134* (**2007**): 3763, https://doi.org/10.1242/dev.011270.

[28] B. Abelson, D. Sun, L. Que, et al., "Sex differences in lower urinary tract biology and physiology," *Biology of Sex Differences 9* (**2018**): 45.

[29] S. K. Sahu, I. Tamadon, B. Rosa, P. Renaud, A. Menciassi, "A Spring-Based Inductive Sensor for Soft and Flexible Robots," *IEEE Sensors Journal 22* (**2022**): 19931.

[30] K. Lee and J. Han, "Analysis of the urine flow characteristics inside catheters for intermittent catheter selection," *Scientific Reports 14* (**2024**): 13273, https://doi.org/10.1038/s41598-024-64395-9.

[31] S. W. Lee and J. H. Kim, "The significance of natural bladder filling by the production of urine during cystometry," *Neurourology and Urodynamics 27* (**2008**): 772, https://doi.org/10.1002/nau.20584.

[32] J. W. N. C. Huang Foen Chung and R. van Mastrigt, "Age and Volume Dependent Normal Frequency Volume Charts for Healthy Males," *Journal of Urology 182* (**2009**): 210, https://doi.org/10.1016/j.juro.2009.02.113.

[33] A. Golgouneh and L. E. Dunne, "A Review in On-Body Compression Using Soft Actuators and Sensors: Applications, Mechanisms, and Challenges," *IEEE Reviews in Biomedical Engineering 17* (**2024**): 166, https://doi.org/10.1109/RBME.2022.3220505.

[34] N. B. Guerra, N. Brizuela Guerra, N. A. Corbellini Henckes, et al., "Biomedical applications of natural rubber latex from the rubber tree Hevea brasiliensis," *Materials Science and Engineering: C 36* (**2021**): 351.

[35] G. E. Papanikolaou, D. N. Varvarousis, G. S. Markopoulos, et al., "Early Systemic Immune Response to Silicone Breast Implants Analyzed by Flow Cytometry," *Cureus 17* (**2025**), https://doi.org/10.7759/cureus.78500.

[36] A. Cardona, V. Iacovacci, T. Mazzocchi, A. Menciassi, and L. Ricotti, "Novel Nanostructured Coating on PDMS Substrates Featuring High Resistance to Urine," *ACS Applied Bio Materials 2* (**2019**): 255.

[37] T. Mazzocchi, G. Lucarini, I. Roehrer, A. Menciassi, and L. Ricotti, "PDMS and DLC-coated unidirectional valves for artificial urinary sphincters: Opening performance after 126 days of immersion in urine," *Journal of Biomedical Materials Research - Part B Applied Biomaterials 110* (**2022**): 817.

[38] P. Singha, J. Locklin, and H. Handa, "A review of the recent advances in antimicrobial coatings for urinary catheters," *Acta Biomaterialia 50* (**2017**): 20.

[39] L. Song, X. Deng, D. Xie, et al., "Suctioning Flexible Ureteroscopy With Automatic Control Of Renal Pelvic Pressure: A Porcine Model," *Journal of Urology 195* (**2016**): e782, https://doi.org/10.1016/j.juro.2016.02.813.

[40] F. A. Hassani, G. G. Gammad, R. P. Mogan, et al., "Design and Anchorage Dependence of Shape Memory Alloy Actuators on Enhanced Voiding of a Bladder," *Advanced Materials Technologies 3* (**2018**): 1700184.

[41] G. Ballardini, I. Tamadon, D. Guarnera, et al., "Controlling and powering a fully implantable artificial pancreas refillable by ingestible pills," *2023 45th Annual International Conference of the IEEE Engineering in Medicine & Biology Society (EMBC)*, (IEEE, **2023**), https://doi.org/10.1109/EMBC40787.2023.10340006.

[42] V. Iacovacci, I. Tamadon, E. F. Kauffmann, et al., "A fully implantable device for intraperitoneal drug delivery refilled by ingestible capsules," *Science Robotics 6* (**2021**): eabh3328.

[43] J. Thimot and K. L. Shepard, "Bioelectronic devices: Wirelessly powered implants," *Nature Biomedical Engineering 1* (**2017**): 0051, https://doi.org/10.1038/s41551-017-0051.

[44] F. Semproni, V. Iacovacci, S. Musco, S. Onorati, M. Ibrahimi, and A. Menciassi, "A fully implantable sensorized artificial urinary bladder to restore continence and fullness monitoring," *APL Bioengineering 9* (**2025**). https://doi.org/10.1063/5.0278500.

© 2025 The Author(s). Advanced Intelligent Systems published by Wiley-VCH GmbH

26404567, 2026, 2, Downloaded from https://advanced.onlinelibrary.wiley.com/doi/10.1002/aisy.202500516 by Veronica Iacovacci - UNIVERSITY OF ESSEX , Wiley Online Library on [24/06/2026]. See the Terms and Conditions (https://onlinelibrary.wiley.com/terms-and-conditions) on Wiley Online Library for rules of use; OA articles are governed by the applicable Creative Commons License